



Original Article

Effective regeneration of rat sciatic nerve using nanofibrous scaffolds containing rat ADSCs with controlled release of rhNGF and melatonin molecules for the treatment of peripheral injury model

Jincheng Zhang, Hengan Ge, Jun Li, Liyang Chen, Jiaqi Wang, Biao Cheng*, Zhitao Rao

Department of Sports Medicine, Tongji Hospital, School of Medicine, Tongji University, 389 Xincun Road, Putuo, Shanghai 200065, PR China

ARTICLE INFO

Article history:

Received 16 March 2023

Received in revised form

6 June 2023

Accepted 13 June 2023

Keywords:

Peripheral nerve

Nerve regeneration

Stem cells

Nanofibrous matrix

In vivo rat model

ABSTRACT

Different therapeutic strategies have been designed and developed for the repair and regeneration of peripheral nerve injury (PNI) tissue as a result of advancements in tissue engineering and regenerative medicine. Due to its versatility, controlled delivery and administration of multifunctional therapeutic agents can be regarded as an effective strategy in treating nerve injury. In this study, melatonin (Mel) molecules and recombinant human nerve growth factor (rhNGF) were loaded on the surface and in the core of polycaprolactone/chitosan (PCL/CS) blended nanofibrous scaffold. To simulate the *in vivo* microenvironment, a dual-delivery three-dimensional (3-D) nanofibrous matrix was developed and the *in vitro* neural development of stem cell differentiation process was systematically examined. The microscopic technique with acridine orange and ethidium bromide (AO/EB) fluorescence staining method was used to establish the adipose-derived stem cells (ADSCs) differentiation and cell–cell communications, which demonstrated that the effective differentiation of the ADSCs with nanofibrous matrix. As investigated observations, ADSCs differentiation was further evident through cell migration assay and gene expression analysis. According to the biocompatibility analysis, the nanofibrous matrix did not trigger any adverse immunological reactions. Based on these characteristics, a 5-week *in vivo* investigation examined the potential of the developed nanofibrous matrix in the regeneration of sciatic nerve of rats. Additionally, compared to the negative control group, the electrophysiological and walking track analyses demonstrated improved sciatic nerve regeneration. This study demonstrates the nanofibrous matrix's ability to regenerate peripheral nerves.

© 2023, The Japanese Society for Regenerative Medicine. Production and hosting by Elsevier B.V. This is an open access article under the CC BY-NC-ND license (<http://creativecommons.org/licenses/by-nc-nd/4.0/>).

1. Introduction

The condition of PNI is a typical medical complication that frequently causes prolonged deterioration of motor and sensory actions and possibly leads to permanent disability by interfering with the brain's capacity to communicate with specific muscles and organs [1,2]. End-to-end microsurgery is typically accepted as a successful therapeutic option for PNI with a small defect gap (<5 mm). Nevertheless, for chronic PNI with a big defect gap (>5 mm), the body's ability to regenerate itself is severely constrained, and an effective form of implant is required to bridge the

nerve gap in order to stimulate axonal regrowth function and functional recovery [3]. The potential implants containing regenerative components like cells and an extracellular matrix in their microenvironment could provide favourable regeneration efficiency to nerve regeneration, autografting, a typical treatment for peripheral nerve injury, demonstrates a high therapeutic impact in the tissue engineering applications [4]. Due to the limited availability of donors and the potential benefit of neuromas at the site where the donor tissue was removed, an alternate non-invasive treatment is necessary [5].

The utilization of nerve guidance conduits (NGCs) as an alternative therapy for the regeneration of peripheral nerves has been the subject of recent researches. An NGC combines the biological and topological features of the scaffolding materials to create an effective microenvironment for nerve repair while suppressing the invasion of inflammatory tissues by enclosing the area of the nerve

* Corresponding author.

E-mail address: 13681973702@sina.cn (B. Cheng).

Peer review under responsibility of the Japanese Society for Regenerative Medicine.

defect with a tubular structure [6]. According to previous research, topological signals from aligned nanofibers made as a framework for the NGC by electro-spinning can regulate regenerative neurons [7]. Instead, the majority of recent scientific researches are focused on developing synthetic or natural polymer-based NGCs [8]. The developed NGC materials are designed to protect the conditions for nerve regeneration, control axon regeneration, retain nerve growth factors (NGFs) in the area designated for wound healing, and significantly resist the invasion of cells that might lead in scarring [9]. The electrospun fiber-based NGCs have greatly attracted the significant attention among the reported systems because of their porous structure walls and potential to show the uniaxially aligned array fibers [10]. A topographical signal to guidance of aligned nanofibers could significantly promote axonal extension during regeneration [11]. Furthermore, the nanofiber conduit can easily integrate with bioactive molecules like growth factors. Peripheral nerve regeneration has been improved by the sustained release of these effectors from the conduit [12].

Growth factors have been found to be particularly effective at accelerating the angiogenesis and neurogenesis of scaffolds. Nerve growth factor (NGF) is an extensively used growth factor type to promote neuronal differentiation [13]. For the majority, NGF has indeed been encapsulated or introduced to culture medium together with other tissue-engineering scaffolds to influence neural tissue repair [14]. For a controlled release of the growth factor from the matrix, Lee et al. disclosed loaded NGF in a fibrin matrix [15]. The axonal growth of the neural cells was greatly improved in a dose-dependent manner when this matrix was used to bridge peripheral nerve deficits [16]. In a different investigation, NGF was made physically immobile on cover slips to encourage the growth of pheochromocytoma cells [17]. The potential choice to be used as biological elements in a nerve conduit is adipose-derived stem cells (ADSCs). Because differentiation of ADSCs promisingly secrete growth factors, help to form myelin, and significantly improve nerve repair, which were therapeutically employed to stimulate nerve tissue repair [18]. Neural stem cells (NSCs) are type of stem cells that could effectively develop into neurons or glial cells [19]. The recent reports stated that many complications of acute peripheral nerve injuries that are promisingly treated by NSC implantation therapy. The brain is the main source of NSCs, which is why neuroblastoma formation is related with a higher rate [2]. The quantity of ADSCs obtained per unit of adipose tissue is substantially larger than with other forms of stem cells, and ADSCs can be obtained by common procedures like liposuction. Furthermore, ADSCs can be converted into NSCs by mixing an appropriate medium with equal amounts of epidermal growth factor (EGF) and fibroblast growth factor (FGF) [20,21]. ADSCs have more potential for differentiation and proliferation than other mesenchymal stem cells [22]. The nanofibrous matrix must be used to completely fill the nerve conduit in order to achieve a uniform distribution of cells throughout the conduit and optimise the transmission of r-ADSCs. The prepared nanofibrous matrix must have certain features including maintaining the cells, not interfering with the axonal growth channel into the conduit lumen, being consistent with cell proliferation, and continuing to be alive [23]. The pineal gland is responsible for the majority of the secretion of melatonin molecules, an endogenous indoleamine hormone that plays a critical role in the control of circadian rhythms. Importantly, the melatonin molecules play a preventive effect in many biomedical therapies including myocardial infarction, hypertension, diabetic cardiomyopathy, and heart failure. Melatonin's anti-inflammatory, anti-oxidative, and anti-apoptotic qualities are responsible for its positive benefits on disorders and regenerative therapies [24,25].

In the present investigation, we designed and constructed a blended CS/PCL nano-fibrous scaffolds for rat sciatic nerve

regeneration. The hydrogel patterning procedure was used to connect the different layers that made up the blended nanofibrous scaffolds. Importantly, blended CS/PCL biodegradation rates provided the controlled release of multiple growth factors in a variety of patterns that provided spatiotemporal biochemical cues. After being covered with rhNGF containing melatonin and encapsulated on the inner surfaces of blended nanofibrous nerve conduits, the electrospun nanofiber materials were transformed into nerve conduits. Then, r-ADSCs were injected into a nanofibrous conduit that had been implanted in a transected sciatic nerve rat model while being loaded with fibrin gel. *In vivo* studies, such as behaviour and attitude and biological tests, were performed in order to demonstrate the successful regeneration of neural tissue at the site of the injured sciatic nerve. This was done after it was confirmed that the multi-layered scaffolds had been successfully constructed and had the capability to regulate the release behavior of multiple growth factors.

2. Materials and methods

2.1. Preparation of PCL/chitosan blended solution for nanofibrous scaffolds

A PCL solution (10 wt%) was made by dissolving bare PCL (MW = 80,000; Sigma Aldrich, USA) in 2,2,2,-trifluoroethanol, and then 5 wt% of chitosan powder (85% deacetylated, Sigma Aldrich, St. Louis, MO) dissolved in trifluoroacetic acid to prepare CS solution. Chitosan and PCL solutions were blended in a 40:60 ratio and vortexed to create a functional PCL-CS blended solution just before electrospinning. This solution ratio has previously been optimised and shown to yield homogenous nanofibers that are stable in both cell culture medium and aqueous solutions. The chitosan and PCL solutions were diluted to 1 and 1.7 wt%, respectively, for spin-coating of the 2-D films, and blended at a ratio of 40:60.

2.2. Fabrication of melatonin and rhNGF loaded blended PCL-CS nanofibers

The disposable syringe (3 mL size) with a 0.5 mm diameter tip was taken with about 2 mL of the prepared chitosan-PCL solution to fabricate electrospinning nanofibers. Setting the syringe's tilt angle allowed the solution to be supplied by gravity. The syringe tip was placed in 20 cm away from a fiber-collecting disc and 25 cm from the horizontal area. The solution was charged at a voltage of 22 kV. For the objective of collecting randomly oriented and aligned nanofibers, respectively, the PCL/CS solution was spinning towards either a 200 rpm revolving grounded drum or two connected consecutive electrodes. Spin-coating the diluted PCL-CS solution at 1000 rpm for 1 min on a coverslip with a 10 mm diameter formed 2-D PCL-CS nanofibrous films. To fabricate Mel molecules and rhNGF loaded nanofibrous scaffolds, 1 mL of rhNGF (10 µg/mL) and Mel in PBS medium was blended with PCL/CS solution. The samples were neutralised with ammonium hydroxide (14%) for 5 min, then thoroughly rinsed with DI water to eliminate any remaining acids from the PCL-CS solution base. Prior to cell seeding, the scaffolds were sterilised by immersing in ethanol (100%) for at least 1 h and then being rinsed with DI water.

2.3. Characterization of blended nanofibers

The scanning electron microscope (SEM) was used to examine the morphology of the prepared PCL-CS nanofibrous scaffolds. Prior to morphological imaging with a JEOL 7000F SEM (JEOL Ltd., Japan) at an accelerating voltage of 5–10 kV, the samples were sputter-coated with gold for 30 s at 18 mA. The nanofibrous diameter

size of the 2-D nanofibers was measured for 100 number of individual fibers using ImageJ software. A versatile uniaxial nanoscale tensile tester that was created in our laboratory was used to assess the tensile characteristics of prepared PCL-CS nanofibers. PCL-CS nano-fiber specimens (10 mm gauge length, 3 mm width) were placed into spring-loaded grips that had surfaces made of fine grit sandpaper, and then the specimens were secured with glue in preparation for tensile tests. The tests were run to fracture at room temperature (25 °C) with the strain rate set to 100 nm/min. Each sample's thickness was determined using SEM at five separate places, and the mean value was used to calculate the stress.

2.4. Study of encapsulation efficiency of rhNGF in blended nanofibers

According to the dissolution of PCL-CS scaffolds encapsulating rhNGF in a 1 mL dichloromethane/PBS (1:1) solution with nanofibrous scaffolds (20 mg) and experiments performed in triplicate, the rhNGF loading level and encapsulation efficiency in the PCL-CS nanofibers were evaluated. Phase transfer would result from this, moving the CS and NGF to the aqueous phase while the PCL moved to the organic phase. After being vortexed for 1 min, the mixture was centrifuged at 7000 rpm for 10 min. After separation, the supernatant was taken out and put through an analysis utilising an NGF ELISA kit and the Bio-Rad assay kit. Triplicate tests were performed on each sample. The ratio of rhNGF loaded, estimated from the supernatant, to the total rhNGF supplied to the PCL-CS during scaffold construction was used to calculate the entrapment efficiency.

2.5. *In vitro* release analysis of rhNGF

The rhNGF@PCL-CS nanofibers were split into small (1 × 1 cm) pieces, added to 1 mL of serum-free RPMI medium culture supplemented with fungizone (0.01%) and penicillin-streptomycin (1%), and then placed on 24-well plates in a water bath under suitable physiological conditions (37 °C). At the pre-set time points (days 1, 4, 7, 14, 21, and 28), release samples were collected, replaced with new medium, and kept at -20 °C until they were required for quantification using an ELISA or PC12 bioassay, in accordance with Aebischer et al [28]. All samples that were obtained and examined underwent statistical significance testing before being reported as mean standard deviation.

2.6. Isolation and expansion of rat ADSCs

All animal-related investigations were carried out in compliance with Isfahan University of Medical Sciences' animal ethics committee's approval and the National Institutes of Health's Guide for the Care and Use of Laboratory Animals. The isolated tissue from Sprague–Dawley (SD) rats was transported to the cell culture lab on ice under sterile settings. Briefly, the inguinal region's adipose tissue was divided into tiny pieces, treated with collagenase type I (0.075%), and agitated for 40 min at suitable condition (37 °C). Each tube of DMEM/F12 (Gibco, USA) medium containing 10% foetal bovine serum (FBS) received the consequent to neutralising enzyme activity. The top layer of fat tissue and the supernatant were removed following centrifugation at 1400 rpm for 10 min. The cell pellet was put into culture flasks with DMEM and 10% FBS before being placed in an incubator with 5% CO₂, 37 °C, and saturated humidity. The media were changed after three to four days, and the cells were sub-cultured until passage four. In this experiment, r-ADSCs, which were obtained from passage 3–4, were used in complete protocol.

2.7. *In vitro* cell compatibility and cell proliferation analysis

The cell survival ability of the PCL-CS NFs, rhNGF@NFs, and rhNGF-Mel@NFs samples was assessed using isolated ADSCs. PCL-CS NFs are considered as a control group. The ADSCs cells were cultivated at 37 °C and 5% CO₂ in DMEM/F12 with FBS (10%), penicillin (5%). Using PBS and trypsin/EDTA, ADSCs cells were sub-cultured every two days until they reached confluence before being employed in the experiment between passages five and ten. The nanofibrous scaffolds were inserted in 6-well plates and disinfected with 70% ethanol before being used to culture the cells on them. Using an MTT assay, a colorimetric assay that gauges the activity of enzymes that convert MTT to formazan dyes, which give purple colours, the scaffolds' *in vitro* biocompatibility was examined. The manufacturer's protocol for the MTT assay was followed. In specifics, a scaffold was seeded with 5 × 10⁴ cells per scaffold, and the scaffold was cultivated in a 6-well culture plate with 5% CO₂ at 37 °C. The culture medium was removed on days 1, 3, 5, and 7 after which the MTT reagent was added to the wells and incubated for an hour. The MTT reagent was then removed, and each well received DMSO. The plates were then agitated for 15 min. The spectrophotometric plate reader was used to calculate the optical density (OD) at 570 nm. Live–dead cell staining (AO/EB) was done to examine the cell proliferation on the nanofibers. After 1, 3 and 7 days of incubation, the culture plate's cell media were discarded, and the live cells were dyed using a live–dead cell staining kit in accordance with the kit's instructions. The cells on the nanofibers were stained and then examined with an Olympus fluorescence microscope (CKX53). The fluorescence intensity was used to semi-quantitatively calculate the number of cells.

The process for cell migration was performed as follows: The upper compartment is filled with 0.1 mL (5 × 10⁴ cells) of ADSCs, which are then incubated there for 24 h at 37 °C. Non-migrated cells were removed from the upper chamber using a cotton swab and then washed in water. Migrated cells were then fixed in 4% paraformaldehyde and stained for 10 min with crystal violet (0.1%). Next, a bottom surface count was performed using an inverted microscope. Each sample underwent the titration three times, with the results being averaged. The treatment groups were concealed from the researcher who carried out the cell counts.

2.8. Encapsulation of ADSCs on prepared NFs

The identical procedure as stated in the section 2.7 was used to load ADSCs onto the rhNM@NFs. The cell density was increased to 2 × 10⁵/mL to improve loading efficiency. Before use, the cells were grown on the NFs for two days. The cells were stained with a live–dead cell staining kit and seen under a fluorescence microscope to study the cells on the NFs in a 2D image (CKX53, Olympus, Japan).

2.9. Animal care and surgical protocol

The Institutional Animal Research Ethics Committee of Tongji University granted its approval for this study, which was conducted strictly in accordance with the guidelines outlined in the Association for Assessment and Accreditation of Laboratory Animal Care International's guideline. Adult Sprague–Dawley (SD) rats (male: 280 ± 30 g) were employed in this study in following the established protocols. The animal chamber was maintained at suitable temperature conditions around 24 ± 3 °C with 40–60% humidity and electronically illuminated from 8:00 a.m. to 8:00 p.m. Ketamine hydrochloride (1.15 μL/g) and xylazine hydrochloride (0.5 μL/g) were used to anaesthetize the SD rats. Rats' left sciatic nerves were exposed before being clamped for 10 s with a 100 g force

micro clamp (jaw width = 2 mm). The nanofibrous scaffold ($10 \times 15 \text{ mm}^2$) wrapped the damaged sciatic nerves. With the scaffold, we bandaged the crushed nerve three times. The muscle and skin were closed with a running suture made of polyglactin 3/0 (Vicryl®) following the injury and scaffold implantation.

2.10. Histological observations

The animals were sacrificed with a high dose of pentobarbital for histology investigation. At frequent intervals of 2, 4, 6, and 12 weeks, the implant was removed and preserved in PFA (4%) for 24 h. The dehydrated tissue sections were paraffin embedded, and the proximal, middle, and distal segments were sliced into thin slices measuring 10 μm both longitudinally and transversely. To explore the nerve anatomy, these sections were stained with H&E staining afterwards deparaffinized and rehydrated.

2.11. Animal behaviour testing

Following sciatic nerve damage, all SD rats were exposed to a sequence of behavioural assessments. When the left hindlimb locomotor activity returned, it was viewed as evidence that the sciatic nerve lesion had sufficiently healed and had regained its functional capacity. This recovery was tracked by examining the free-walking pattern, a technique that had been used in a prior study. In this experiment, SD rats were put on a track that was 500 mm long, 100 mm wide, and ended in a dark box. The SD rats were then permitted to walk after having a dark dye painted on the plantar surface of their hind paws. The sciatic functional index (SFI) was determined using the rat footprints. Three measurements were made from the footprints: the print length (PL), which is the measurement from the heel to the third toe, the toe spread (TS), which is the measurement from the first to the fifth toe, and the toe spread (ITS), which is the measurement from the second to the fourth toe (ITS). The experimental (E) and normal (N) sides were used to collect data for all three measurements. The equations were changed to reflect the measured values, and the SFI values were calculated ($n = 12$). A basal pain sensitivity was assessed both before and after the scaffolds were implanted as an extra behavior investigation. On a raised wire grid, SD rats were positioned. The plantar surface of the hind paw was stimulated with a set of von Frey hairs to alleviate mechanical allodynia. In this investigation, a dynamic plantar esthesiometer was used to quantify the mechanical paw withdrawal threshold (PWT) (Ugo Basile, Varese, Italy). The threshold was defined as the minimal force required to cause a quick withdrawal reaction (1–50 g in 50 s). The mechanical stimulus was automatically withheld when the rat retracted its hind paw ($n = 12$).

2.12. Statistical analysis

Using SPSS 23 statistical software (IBM, NY), the results of the behavioural studies and quantitative analyses were statistically assessed by one-way ANOVA. $P < 0.05$ was used to state as a significant difference between groups, while $P < 0.001$ was used to define a highly significant difference.

3. Results and discussion

During electrospinning process, a variety of factors affect fibre morphology and diameter size. The nanofiber shape is significantly influenced by the emulsion's composition and contents. The electric forces in the spinning process may cause some of the emulsion droplets to fragment into smaller droplets if they are noticeably elongated. When the solvent evaporates, the emulsion jet generates

nanoscale fibers with integrated drug molecules and/or proteins. Fig. 1 displays SEM microscopic images of the various electrospun nanofiber scaffold types with different contents. The nanofibers are homogeneous, have smooth surfaces, and have a fibrous structure with no beads at the nanoscale. The PCL, PCL-MCS, and rhNGF@PCL-MCS nanofiber scaffolds had fibre diameters in the ranges of 160–240 nm, 180–260 nm, and 160–320 nm, respectively (Fig. 1). This study demonstrates that pure PCL and PCL-MCS nanofibers made using the same electrospinning method had larger diameters than rhNGF-encapsulated PCL-MCS nanofibers. Tensile tests were employed to evaluate the mechanical characteristics of the electrospun fabricated PCL-MCS NFs and rhNGF-PCL-MCS as shown in Fig. 2. The characteristic stress–strain graphs (Fig. 2a) indicated that each sample of nanofibers acted similarly, exhibiting linear elastic response followed by plastic distortion until breakdown. Both the PCL-MCS NFs and rhNGF@PCL-MCS had significantly higher Young's moduli (Fig. 2b) and ultimate tensile strengths (Fig. 2c) than pure PCL nanofiber, but lower ultimate stresses (Fig. 2d). This revealed that, because to the high rigidity and high tensile strength of melatonin-loaded chitosan molecules, the addition of Melatonin-CS enhanced the stiffness and strength of as-prepared NFs but also partially lost the NFs' extensibility. Additionally, we discovered that the addition of rhNGF significantly boosted the PCL-ultimate MCS's strength while correspondingly reducing its ultimate strain.

The percentage of rhNGF that was successfully encapsulated in PCL and PCL-MCS nanofibers was $96.15\% \pm 2.30\%$ and $70.45\% \pm 1.15\%$, respectively. The findings indicate that the blended nano-fiber had a substantial impact on the efficiency of encapsulation. More rhNGF were lost during the preparation of PCL nanofibers alone, which reduced the encapsulation effectiveness of bare PCL nanofibers. The total content of encapsulated rhNGF in two groups (PCL NFs and PCL-MCS NFs) all exhibited an obvious improvement with the increasing in rhNGF reaction concentration as shown in Fig. 3a. At the same concentration, the loading content of PCL-MCS NFs group had substantially greater than PCL NFs group. ELISA assay method was used to evaluate the cumulative release patterns of rhNGF from PCL and PCL-MCS NFs at each time point (Fig. 3b). It was observed that PCL NFs had released rhNGF in bursts at a faster rate than PCL-MCS NFs within four days. The long-term release profile demonstrated that as incubation days were increased, the release of rhNGF for both NFs slowed until it reached to a complete standstill. Within the first four days, about $32.13 \pm 1.2\%$ of rhNGF was rapidly released; after that, the release kinetics slowed and came to a release rate at $55.20 \pm 2.5\%$ on the tenth day. The release of rhNGF showed that a medication or protein might be successfully delivered over time using a porous and nanofibrous morphological framework.

Fig. 4a illustrates cell compatibility behaviour by MTT assay method, in which absorbance values are significantly proportional to the number of viable cells introduced to the prepared samples, was used to assess the *in vitro* biocompatibility of the fabricated nanofibrous scaffolds. It is obvious that the ADSCs were effectively viable and could proliferated when increasing incubation time (days) in all nanofibrous scaffold groups. On developed PCL-MCS nanofibrous matrix, more than 90% of ADSCs continued to viable and migrated after 7, 14, and 21 days of *in vitro* culture. At days 1, 4, 7, 14, and 21, MTS assays were used to determine the proliferative potential of ADSCs sown on various nanofibrous scaffolds. The proliferation of ADSCs did not significantly change between the first and fourth day, as seen in Fig. 4b. After 7 days of cell seeding, ADSC proliferation on PCL-MCS NFs and NGF@PMCS NFs groups is significantly efficient than that of the PCL NFs group. The proliferation of cells seeded on the PCL group was less than that in the other three groups on days 14 and 21. Proliferation of ADSCs was

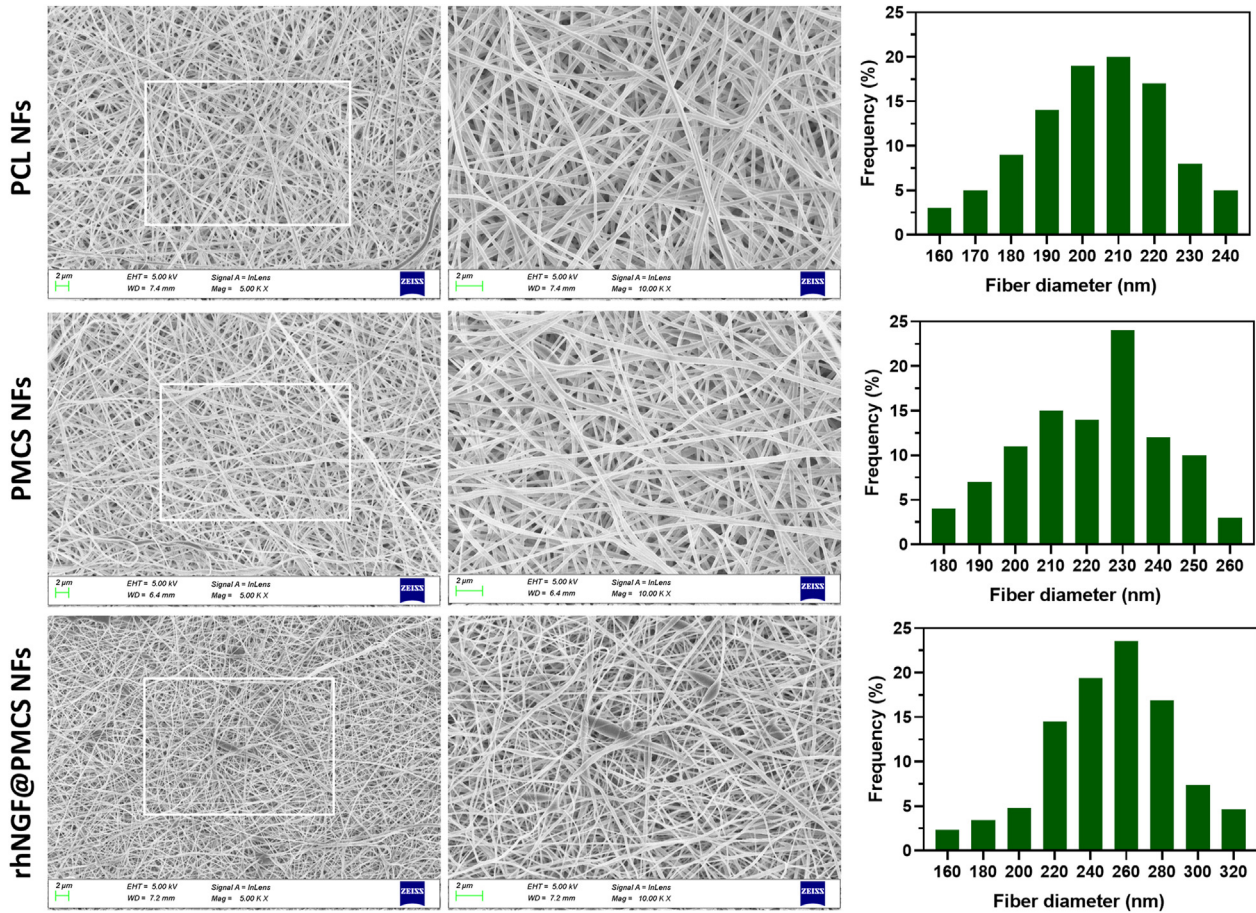


Fig. 1. The morphological observation (SEM images) of nanofibers as well as measurements of nanofibers size distribution of electrospun PCL NFs, PMCS NFs and rhNGF@PMCS NFs; the scale bar is 2 μm.

sown on NGF@PMCS NFs on day 21 is greatly higher than that of other comparative groups. Meanwhile, transwell migration technique is used to evaluate how rhNGF influences ADSCs cell migration ability as exhibited in Fig. 5a. When rhNGF is added to fabricated NFs, it can significantly increase the potential of ADSC cells to migrate across nanofibrous membranes. When compared to other NFs samples, the majority of these cells move through nanofibrous membranes at rhNGF loaded PMCS NFs. However, as demonstrated in Fig. 5b, without the addition of rhNGF, the capacity of ADSCs cells to migrate is gradually reduced. The current findings agree with previous research [26]. The specialized purposes of FDA approved PCL and chitosan, the biocompatible polymeric materials used in this study to fabricate nanofibrous scaffolds for tissue engineering and drug delivery applications. The fabricated PCL-MCS nanofibrous scaffold exhibited potential cell proliferations during the first seven days of culture and was also biocompatible as anticipated (Fig. 4a). Since it is well known that the electrospun nano-fibrous framework accurately reflects the extracellular matrix and facilitates the cell attachment, migration, and proliferation of cells more effectively, the cells were planted on and grew within the fibrous structure.

The quantitative technique (qRT-PCR) was used to evaluate the gene expression of different nanofibrous scaffolds encapsulated with ADSCs and rhNGF molecules, respectively. Fig. 6 displays the gene expression levels for -actin, GFAP, MAP2, NSE and Tuj1 for 4, 7, and 14 days. At 7 and 14 days, the PCL NFs group had significantly lower expression levels of β-actin, GFAP, MAP2, and Tuj1 than the other three groups. At day 14, the MAP2, NSE, and Tuj1 expression

levels in the ADSCs/rhNGF@PCMS NFs group were significantly greater than those in the rhNGF@PCMS NFs and PCMS NFs groups as shown in Fig. 6. According to qRT-PCR results (Fig. 6), at three separate time durations (7, 14 and 21 days), there were significant changes in the mRNA expression levels of the particular markers for neuronal development. Although we did not quantify how much of the bioactivity was lost due to the alteration, this finding clearly indicated that the conjugated rhNGF and ADSCs demonstrated good bioactivity on the nanofibrous scaffold. In addition to rhNGF, which is frequently used to promote neuronal differentiation, ADSCs have also been proven to promote neuritic development and to promote neuroprotection. Since ADSCs further enhanced rhNGF's ability to induce neuronal differentiation, the ADSCs/rhNGF loaded nanofibrous group displayed statistically significant greater expression levels of the markers for neuronal differentiation than the other groups (Fig. 6).

We initially examined motor function in a rat injury model of biceps femoris injury to the sciatic nerve to assess whether the local delivery of rhNGF and ADSCs from the developed nanofibrous scaffolds at the site of injury was efficient in regeneration of peripheral nerve injury. The sciatic functional index (SFI), a robust approach to measure the restoration of foot muscle innervation, was used to assess motor recovery following sciatic nerve damage. Fig. 7a displays the SFI values for all four groups at 0, 1, 2, 3, and 5 weeks following the implantation of nanofibrous scaffolds. All groups' SFI values increased over time. After two weeks, the ADSCs/rhNGF@PMCS NFs group and rhNGF@PMCS NFs had more superior progressive improvements than the rhNGF and the control groups.

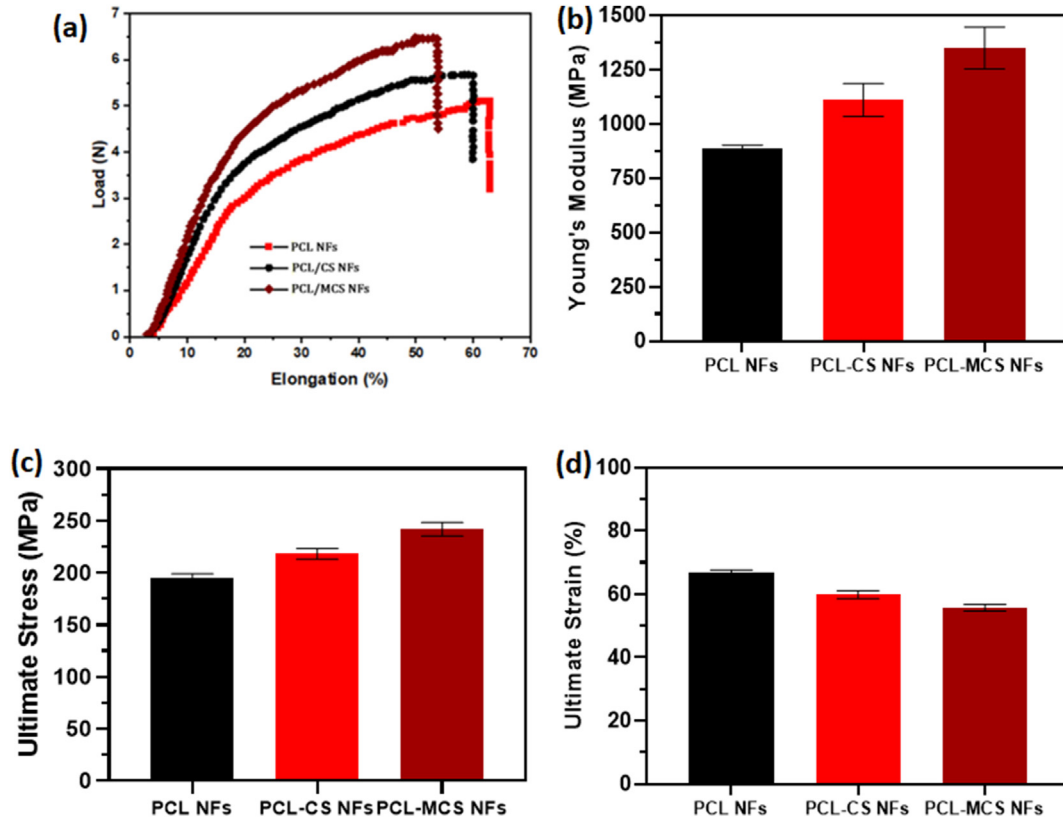


Fig. 2. Mechanical characterization of prepared nanofibrous scaffolds; (a) stress–strain behaviour, (b) young modulus, (c) ultimate strength and (d) ultimate strain.

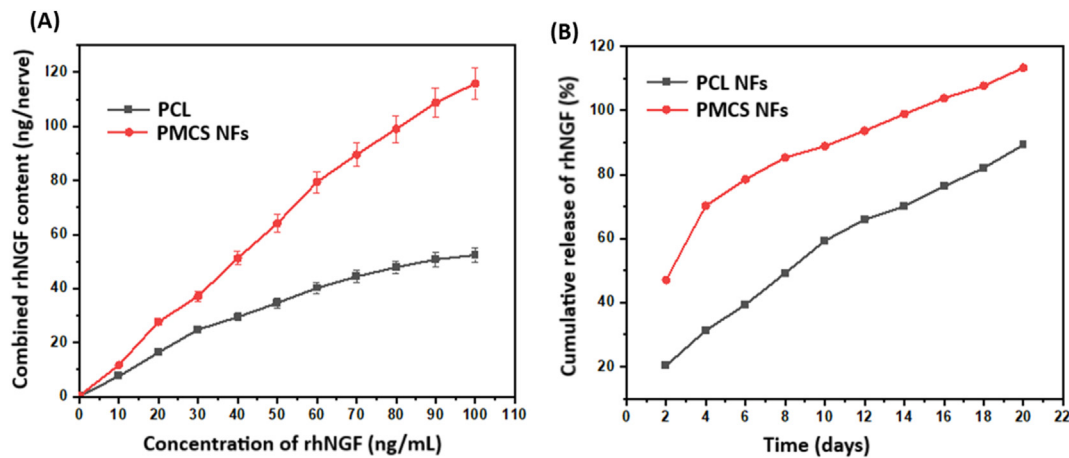


Fig. 3. (A) rhNGF content of PCL NFs and PMCS NFs at different reaction concentration and (B) long term *in vitro* release of rhNGF from PCL NFs and PMCS NFs.

At all points following implantation, it was determined that the improvements in the ADSCs encapsulated NFs group's results relative to the control and rhNGF groups were statistically significant. Overall, there was a highly significant difference between the ADSCs/rhNGF@PMCS NFs and the control and other groups in the SFI values at weeks 4 and 5. There was a significant difference between the ADSCs/rhNGF@PMCS NFs and control groups for the outcome after 5 weeks.

Subsequently, the pain signal induced by a touch stimulation employing von Frey hairs was used to assess the sensory function. As seen in Fig. 7b, all groups have seen an increase in ipsilateral mechanical allodynia after injured sciatic nerve with implantation

of developed nanofibrous scaffolds, and similar trends could be seen with SFI data (Fig. 6a). After two weeks, the rhNGF@PMCS NFs and control groups exhibited threshold values that were considerably lower than the ADSCs/rhNGF@PMCS NFs. There was no discernible difference between these two groups for any of the testing times, despite the fact that the rhNGF@PMCS NFs group likewise had greater values than the ADSCs encapsulated NFs group. These two behavioural experiments revealed that the SCI regeneration was not improved by the bare PCMS NFs without simultaneous loading of rhNGF and ADSCs. Due to the more consistent release of rhNGF and the bio-activity of ADSCs, PMCS NFs have exponential activity at the same time and produced

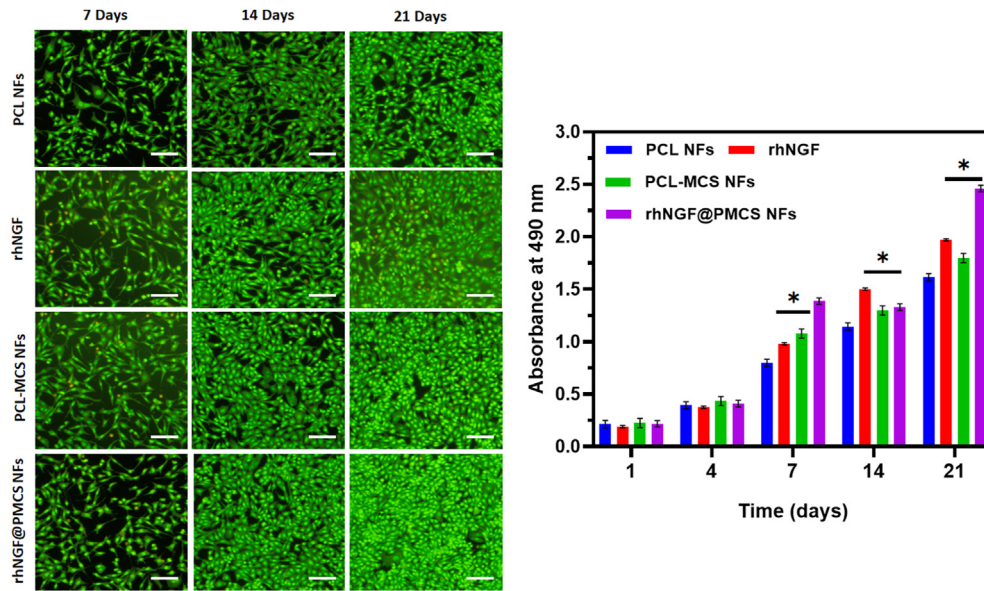


Fig. 4. (A) Live/dead staining observations of ADSCs cultured on different nanofibrous scaffolds at different incubation period (7, 14 & 21 days) *in vitro*. AO/EB dual staining labelled with cells to show green/red fluorescence to visualize live/dead cells. (B) *In vitro* cell viability of ADSCs treated with different nanofibers (PCL NFs, rhNGF, PCL-MCS NFs and rhNGF@PCL-MCS NFs) at different incubation time from 1 to 21 days. Scale bars: 50 μ m.

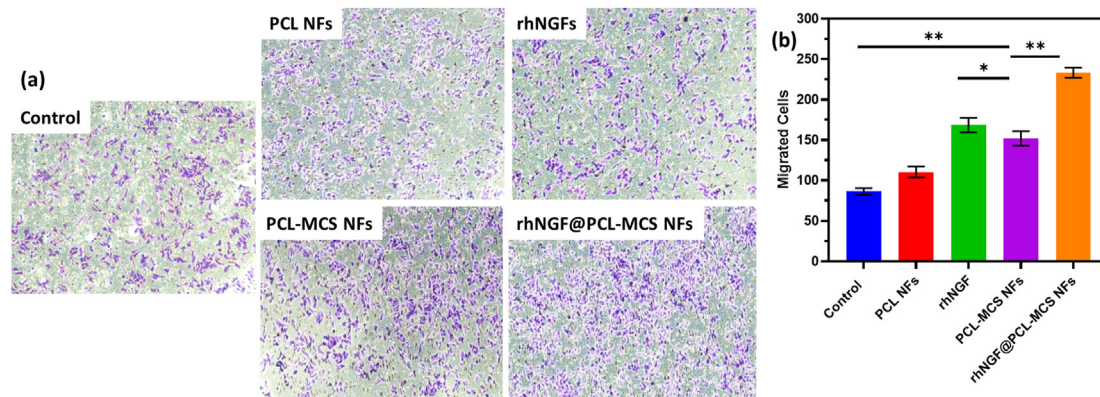


Fig. 5. (A) The ADSCs migration ability after treated with PCL NFs, rhNGF, PCL-MCS NFs and rhNGF@PCL-MCS NFs observed by transwell migration assay and (B) quantitative measurement of migrated cells through different nanofibers.

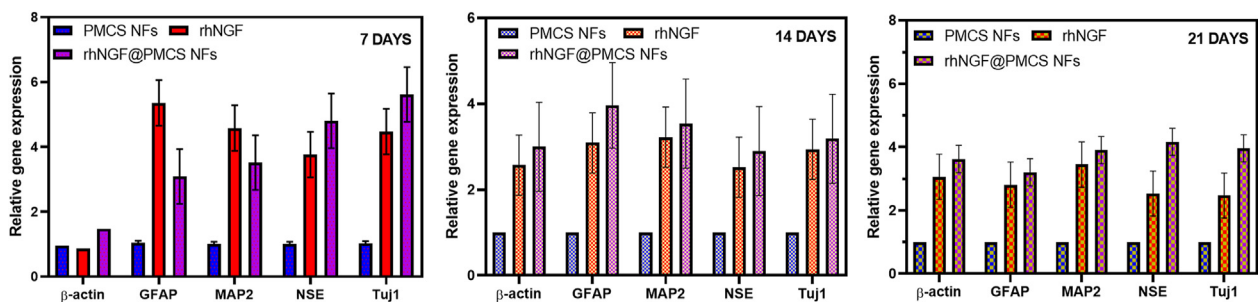


Fig. 6. Quantitative observations of the gene expression (β -actin, GFAP, MAP2, NSE and Tuj1) in ADSCs after seeded on developed nanofibrous scaffolds at different incubation time (7 days, 14 days and 21 days). Data are expressed as mean \pm SD (n = 3).

substantially better results than the control. The quantitative measurement of the motor recovery in regeneration of neural tissue regeneration depends on the results of the behavioural analysis [19]. Using the rat as a model animal, we examined mechanical allodynia and SFI for 5 weeks in this investigation. To

examine the impact of controlled release ADSCs and rhNGF to the wounded site, a recovery period of 5 weeks was chosen for the adult rat model's sciatic nerve tissue regeneration. This recovery period was chosen in agreement with the injured short gap (2 mm) model. The SFI has been extensively utilized to evaluate

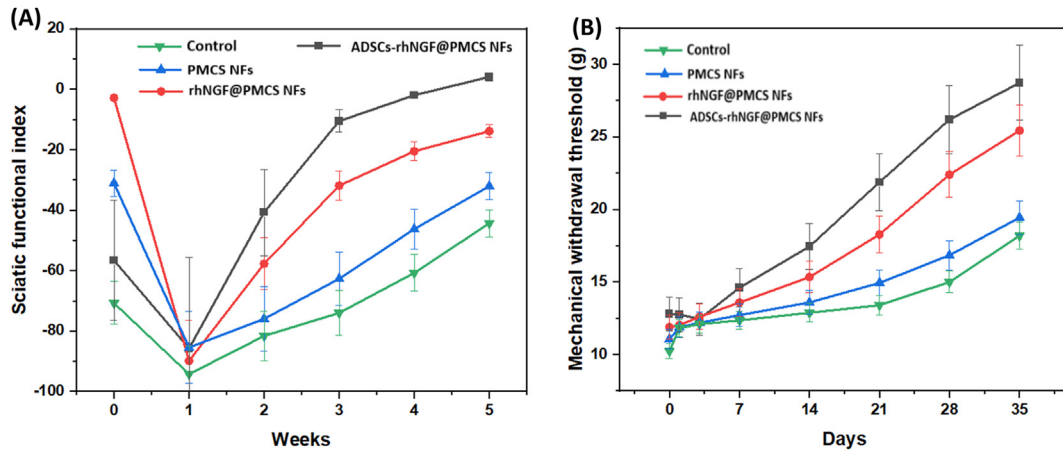


Fig. 7. (A) Sciatic functional index (compression injury) and mechanical allodynia measurement for the control, PMCS NFs, rhNGF@PMCS NFs and ADSCs-rhNGF@PMCS NFs groups from 1 to 5 weeks period.

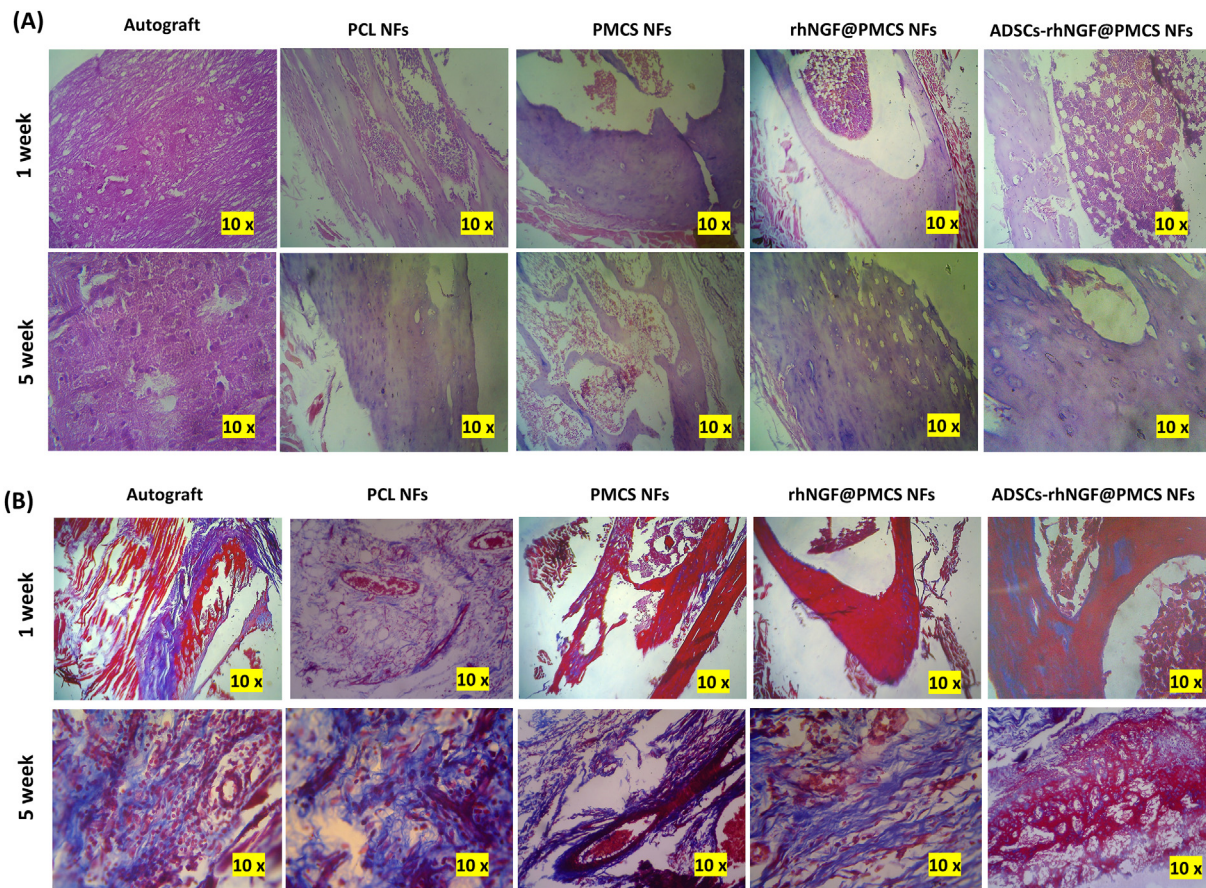


Fig. 8. The histopathological observation of injured sciatic nerve at 1 and 5 weeks after repair. The respective treated sample images of (A) H&E staining and (B) MTS staining of autograft, PCL NFs, PMCS NFs, rhNGF@PMCS NFs and ADSCs-rhNGF@PMCS NFs after transplanted for 1 and 5 weeks. Magnifications: 10x.

the restoration of motor function as a result of the wounded sciatic nerve's regeneration. Due to the animals' tendency to attack their denervated hind limbs following sciatic nerve transection, some previous researches do not advise using SFI for the evaluation of motor function recovery [23]. We used a micro clamp to damage the tissue rather than transecting the sciatic nerve to reduce this concern. The release rate of growth factors had a substantial impact on the neural tissue regeneration, as was noted in the *in vivo* experiments above. The behaviour

experiments show that the PCL NFs and PCL/MCS NFs groups only slightly improved the regeneration of the damaged sciatic nerve in the absence of rhNGF and ADSCs. Conversely, the ADSCs/rhNGF@PMCS NFs group, whose growth factor was delivered gradually, had a much superior recovery than the bare nanofibrous groups in terms of both the SFI value and the mechanical allodynia force. The ADSCs/rhNGF@PMCS NFs were much greater than the rhNGF@PMCS group, as evidenced by the SFI result from week 5 in particular.

After weeks 1 and 5 of post-operation period, the histological morphology changes in the various experimental groups were assessed using H-E staining and Masson's trichrome (MTS) staining methods under microscopic technique as shown in Fig. 8a and b. The autograft group's nerve tissue displayed degradation of myelin sheath and vacuoles in the nerve fibres at one month after post-surgery. Sciatic nerve fibres with vacuoles and an unorganised arrangement were present in the PCL NFs group. The PCL/MCS NFs group, rhNGF@PMCS NFs group, and ADSCs/rhNGF@PMCS NFs group all had better orderly arrangement and much less vacuolation as compared to the PCL NFs group. In comparison to the PCL and PCL/MCS NFs groups, there was higher cell infiltration in the rhNGF@PMCS NFs group and the ADSCs/rhNGF@PMCS NFs group. At three months after surgery, the autograft group's nerve tract and architecture were uniformly normal, and fresh blood vessels were also apparent. In the PCL NFs group, there were more inflammatory cells visible in the spaces between the fibres, the myelin sheath was arranged erratically, and the distribution of fibres was irregular. The PMCS NFs group demonstrated more pronounced cell proliferation, more homogeneous cell distribution, and more new blood vessel creation as compared to the PCL NFs group. The distribution of nerve fibres was much more uniform in the rhNGF@PMCS NFs group than in the PMCS NFs group. The developed rhNGF@PMCS NFs group excelled regeneration performance than the PCL NFs and PCL-MCS NFS group in terms of ADSCs cell proliferation, cell distribution, the arrangement of nerve fibres, and the development of new blood vessels. According to the results of H&E (Fig. 8a) and MTS (Fig. 8b) staining on slices of the gastrocnemius muscle, the ADSCs/rhNGF@PMCS NFs group had the highest healing outcomes at three months of post-operation period. The H&E staining (Fig. 8a) revealed that the ADSCs/rhNGF@PMCS NFs group had the most vasculature at 5 weeks compared to the other groups. The nerve conduit nanofibrous scaffolds' vascularity can provide the ideal milieu for distributing nutrition, oxygen, and a number of neurotrophic agents for nerve regeneration [27]. In addition to angiogenesis, neural stem cells' migratory responses in the rhNGF-releasing nanofibrous scaffolds were also seen during the process of nerve regeneration. Additionally, the ADSCs/rhNGF@PMCS NFs group's results were similar to those of the autograft group according to the MTS stain of the gastrocnemius muscle. The nanofibrous scaffold with rhNGF encapsulation could regulate the proliferation and neural differentiation of ADSCs *in vitro*, fulfilling the requirement of blood vessel formation and nerve regeneration *in vivo*, according to the *in vitro* and *in vivo* experiments as well as the thorough evaluation.

4. Conclusion

The present study established a facile technique for administering rhNGF to PCL/MCS nanofibrous scaffolds. Melatonin molecules were added to the electrospinning solution in a way that increased substantially the biocompatibility of the released rhNGF. For up to 28 days, the bioactivity of rhNGF was properly maintained. The current approach could encourage axon elongation and enhance functional recovery of the rat sciatic nerve by combining rhNGF, ADSCs, and bioactive nanofibrous materials. The nanofibrous nerve conduits have the ability to be employed as a therapeutic material for peripheral nerve injury even though the regeneration efficacy is really only substantially equivalent to autograft.

Declaration of competing interest

The authors declare no competing financial interest.

References

- [1] Guo ZY, Sun X, Xu XL, Zhao Q, Peng J, Wang Y. Human umbilical cord mesenchymal stem cells promote peripheral nerve repair via paracrine mechanisms. *Neural Regen Res* 2015;10:651–8.
- [2] Syu WZ, Hueng DY, Chen WL, Chan JYH, Chen SG, Huang SM. Adipose-derived neural stem cells combined with a cellular dermal matrix as a neural conduit enhances peripheral nerve repair. *Cell Transplant* 2019;28:1220–30.
- [3] Georgiou M, Golding JP, Loughlin AJ, Kingham PJ, Phillips JB. Engineered neural tissue with aligned, differentiated adipose-derived stem cells promotes peripheral nerve regeneration across a critical sized defect in rat sciatic nerve. *Biomaterials* [Internet] 2015;37:242–51. <https://doi.org/10.1016/j.biomaterials.2014.10.009>.
- [4] Samadian H, Maleki H, Fathollahi A, Salehi M, Gholizadeh S, Derakhshankhah H, et al. Naturally occurring biological macromolecules-based hydrogels: potential biomaterials for peripheral nerve regeneration. *Int J Biol Macromol* [Internet] 2020;154:795–817. <https://doi.org/10.1016/j.ijbiomac.2020.03.155>.
- [5] Huang Q, Cai Y, Zhang X, Liu J, Liu Z, Li B, et al. Aligned graphene mesh-supported double network natural hydrogel conduit loaded with netrin-1 for peripheral nerve regeneration. *ACS Appl Mater Interfaces* 2021;13:112–22.
- [6] Yang Z, Yang Y, Xu Y, Jiang W, Shao Y, Xing J, et al. Biomimetic nerve guidance conduit containing engineered exosomes of adipose-derived stem cells promotes peripheral nerve regeneration. *Stem Cell Res Ther* [Internet] 2021;12:1–14. <https://doi.org/10.1186/s13287-021-02528-x>.
- [7] Ikegami Y, Ijima H. Development of heparin-conjugated nanofibers and a novel biological signal by immobilized growth factors for peripheral nerve regeneration. *J Biosci Bioeng* [Internet] 2020;129:354–62. <https://doi.org/10.1016/j.jbiosc.2019.09.004>.
- [8] Alavi M. Antibacterial and wound healing activities of silver nanoparticles embedded in cellulose compared to other polysaccharides and protein polymers. *Cellulose* 2021;28:8295–311.
- [9] Hong MH, Hong HJ, Pang H, Lee HJ, Yi S, Koh WG. Controlled release of growth factors from multilayered fibrous scaffold for functional recoveries in crushed sciatic nerve. *ACS Biomater Sci Eng* 2018;4:576–86.
- [10] Roozbahani F, Sultana N, Fauzi Ismail A, Noupurvar H. Effects of chitosan alkali pretreatment on the preparation of electrospun PCL/chitosan blend nanofibrous scaffolds for tissue engineering application. *J Nanomater* 2013;2013.
- [11] Hu J, Tian L, Prabhakaran MP, Ding X, Ramakrishna S. Fabrication of nerve growth factor encapsulated aligned poly(ϵ -caprolactone) nanofibers and their assessment as a potential neural tissue engineering scaffold. *Polymers (Basel)* 2016;8.
- [12] Kim MJ, Lee JH, Kim JS, Kim HY, Lee HC, Byun JH, et al. Intervertebral disc regeneration using stem cell/growth factor-loaded porous particles with a leaf-stacked structure. *Biomacromolecules* 2020;21:4795–805.
- [13] Xia B, Lv Y. Dual-delivery of VEGF and NGF by emulsion electrospun nanofibrous scaffold for peripheral nerve regeneration. *Mater Sci Eng C* [Internet] 2018;82:253–64. <https://doi.org/10.1016/j.msec.2017.08.030>.
- [14] Tian L, Prabhakaran MP, Hu J, Chen M, Besenbacher F, Ramakrishna S. Coaxial electrospun poly(lactic acid)/silk fibroin nanofibers incorporated with nerve growth factor support the differentiation of neuronal stem cells. *RSC Adv* 2015;5:49838–48.
- [15] Lee AC, Yu VM, Lowe JB, Brenner MJ, Hunter DA, Mackinnon SE, et al. Controlled release of nerve growth factor enhances sciatic nerve regeneration. *Exp Neurol* 2003;184:295–303.
- [16] Raoofi A, Sadeghi Y, Piryaeei A, Sajadi E, Aliaghaei A, Rashidiani-Rashidabadi A, et al. Bone marrow mesenchymal stem cell condition medium loaded on PCL nanofibrous scaffold promoted nerve regeneration after sciatic nerve transection in male rats. *Neurotox Res* [Internet] 2021;39:1470–86. <https://doi.org/10.1007/s12640-021-00391-5>.
- [17] Xue J, Yang J, O'Connor DM, Zhu C, Huo D, Boulis NM, et al. Differentiation of bone marrow stem cells into Schwann cells for the promotion of neurite outgrowth on electrospun fibers. *ACS Appl Mater Interfaces* 2017;9:12299–310.
- [18] Razavi S, Jahromi M, Vatankhah E, Seyedehbrahimi R. Differential effects of rat ADSCs encapsulation in fibrin matrix and combination delivery of BDNF and gold nanoparticles on peripheral nerve regeneration. *BMC Neurosci* [Internet] 2021;22:1–16. <https://doi.org/10.1186/s12868-021-00655-y>.
- [19] Vishnoi T, Singh A, Teotia AK, Kumar A. Chitosan-gelatin-polypropylene cryogel matrix for stem cell differentiation into neural lineage and sciatic nerve regeneration in peripheral nerve injury model. *ACS Biomater Sci Eng* 2019;5:3007–21.
- [20] Zhou LN, Wang JC, Zilundu PLM, Wang YQ, Guo WP, Zhang SX, et al. A comparison of the use of adipose-derived and bone marrow-derived stem cells for peripheral nerve regeneration *in vitro* and *in vivo*. *Stem Cell Res Ther* 2020;11:1–16.
- [21] Sun Y, Chi X, Meng H, Ma M, Wang J, Feng Z, et al. Polylysine-decorated macroporous microcarriers laden with adipose-derived stem cells promote nerve regeneration *in vivo*. *Bioact Mater* [Internet] 2021;6:3987–98. <https://doi.org/10.1016/j.bioactmat.2021.03.029>.

- [22] Sowa Y, Kishida T, Imura T, Numajiri T, Nishino K, Tabata Y, et al. Adipose-derived stem cells promote peripheral nerve regeneration in vivo without differentiation into Schwann-like lineage. *Plast Reconstr Surg* 2016;137:318e–30e.
- [23] Zhou G, Chang W, Zhou X, Chen Y, Dai F, Anwar A, et al. Nanofibrous nerve conduits with nerve growth factors and bone marrow stromal cells pre-cultured in bioreactors for peripheral nerve regeneration. *ACS Appl Mater Interfaces* 2020;12:16168–77.
- [24] Rahim I, Sayed RK, Fernández-Ortiz M, Aranda-Martínez P, Guerra-Librero A, Fernández-Martínez J, et al. Melatonin alleviates sepsis-induced heart injury through activating the Nrf2 pathway and inhibiting the NLRP3 inflammasome. *Naunyn-Schmiedeberg's Arch Pharmacol* 2021;394:261–77.
- [25] Chen G, Deng H, Song X, Lu M, Zhao L, Xia S, et al. Reactive oxygen species-responsive polymeric nanoparticles for alleviating sepsis-induced acute liver injury in mice. *Biomaterials* [Internet] 2017;144:30–41. <https://doi.org/10.1016/j.biomaterials.2017.08.008>.
- [26] Shi ZL, Fan ZY, Zhang H, Li ST, Yuan H, Tong JH. Localized delivery of brain-derived neurotrophic factor from PLGA microspheres promotes peripheral nerve regeneration in rats. *J Orthop Surg Res* [Internet] 2022;17:1–10. <https://doi.org/10.1186/s13018-022-02985-x>.
- [27] Zhao B, Zhao Z, Ma J, Ma X. Modulation of angiogenic potential of tissue-engineered peripheral nerve by covalent incorporation of heparin and loading with vascular endothelial growth factor. *Neurosci Lett* 2019;705:259–64.
- [28] Aebischer P, Schluep M, Déglon N, Joseph JM, Hirt L, Heyd B, et al. Intrathecal delivery of CNTF using encapsulated genetically modified xenogeneic cells in amyotrophic lateral sclerosis patients. *Nature Medicine* 1996;2:696–9.